CORE
Metadata, citation and similar papers at core.ac.uk
Provided by TECNALIA Publications

PM-Assisted Synchronous Reluctance Machine Field Weakening Control for EV and HEV Applications

Elena Trancho, Edorta Ibarra, Antoni Arias, Iñigo Kortabarria, Jonathan Juŕgens, Luca Marengo, Antonio Fricassè, Johannes Gragger
2017 IEEE Transactions on Industrial Electronics. Personal use of this material is permitted.
Permission from IEEE must be obtained for all other uses,
in any current or future media, including reprinting/republishing this material
for advertising or promotional purposes, creating new collective works, for resale or redistribution to servers or lists,
or reuse of any copyrighted component of this work in other works.
DOI: 10.1109/TIE.2017.2748047

***Abstract*—In this manuscript, a novel robust torque control strategy for Permanent Magnet Assisted Synchronous Reluctance Machine drives applied to electric vehicles and hybrid electric vehicles is presented. Conventional control techniques can highly depend on machine electrical parameters, leading to poor regulation under electrical parameters deviations or, in more serious cases, instabilities. Additionally, machine control can be lost if field weakening is not properly controlled and, as a consequence, uncontrolled regeneration is produced. Thus, advanced control techniques are desirable to guarantee electric vehicle drive controllability in the whole speed/torque operation range and during the whole propulsion system lifetime. In order to achieve these goals, a combination of a robust second order current based Sliding Mode Control and a Look-up Table/Voltage Constraint Tracking based hybrid Field Weakening control is proposed, improving the overall control algorithm robustness under parameter deviations. The proposed strategy has been validated experimentally in a full scale automotive test bench (51 kW prototype) for being further implemented in real hybrid and electric vehicles.**

***Index Terms*—Traction motors, machine control, torque control, electric vehicles.**

Manuscript received Month xx, 2xxx; revised Month xx, xxxx; accepted Month x, xxxx. This work was supported in part by the FP7/European Comission under Grant 605075 (SYRNEMO project), by the Government of the Basque Country within the research program ELKARTEK as the project KT4TRANS (KK-2015/00047), by the Ministerio de Economía y Competitividad of Spain within the project DPI2014-53685-C2-2-R and FEDER funds, by the Spanish projects DPI2013-41224-P (Ministerio de Educación) and 2014 SGR 267 (AGAUR). This work has been carried out inside the Research and Education Unit UFI11/16 of the UPV/EHU and supported by the Department of Education, Linguistic Policy and Culture of the Basque Government within the fund for research groups of the Basque University System IT978-16.

(Authors' names and affiliation) E. Trancho is with the Industry and Transport Unit, Tecnalia Research and Innovation, Parque Científico y Tecnológico de Bizkaia, c/ Geldo, Edif. 700, 48160 Derio, Spain (elena.trancho@tecnalia.com). E. Ibarra and I. Kortabarria are with the Department of Electronic Technology, UPV/EHU, C. Rafael Moreno Pitxitxi 3, 48013 Bilbao, Spain. T. Arias is with the Institut d'Organització i Control, Universitat Politècnica de Catalunya, Diagonal, 647, 08028 Barcelona, Spain. J. Juŕgens is with the Institute for Drive Systems and Power Electronics, Leibniz Universität Hannover, 30167, Hannover, Germany. L. Marengo and A. Fricassè are with CRF S.c.p.A, Strada Torino, 50, 10043, Orbassano, Italy. J. Gragger is with the AIT, Austrian Institute of Technology GmbH, Mobility Department, Giefinggasse 2, Vienna, 1210, Austria.

I. Introduction

PERMANENT Magnet Synchronous Machines (PMSMs) have been traditionally considered as appropriate candidates for Electric Vehicle (EV) and, specially, for Hybrid Electric Vehicle (HEV) applications, due to their high power density and high efficiency [1]. However, these technologies require high density magnetic materials to produce the rotor flux, usually sintered neodymium-iron-boron (NdFeB) alloys, and other rare-earth materials, such as dysprosium (Dy), leading to high price, risk of depletion and resource monopoly issues [2], [3]. For these reasons, alternative technologies that do not rely on these PM materials are attracting considerable attention, such as Switched Reluctance Machines (SRMs) [4], [5] and Induction Machines (IMs) [6]. Among them, Synchronous Reluctance Machines (SynRMs) can be highlighted due to their high temperature operation capability, high efficiency, and small [7] (usually ferrite magnets) or eventually non use of PMs [8]. These features make the SynRMs one of the most promising candidates for the next generation of EV and HEV [3]. According to [9], modern ferrite PM-Assisted machines can produce 75 % of the torque of an Interior PMSM for the same size and liquid cooling technology.

A significant amount of research has been carried out in the last years regarding SynRMs and PM-Assisted SynRMs, with special attention on machine design and optimization aspects [10]–[13]. Control aspects have also been studied in the recent literature. In this sense, [14], [15] deal with the high speed control of synchronous machines, in general, and SynRMs, in particular, being this an important aspect for next

generation high speed EV propulsion systems. In [16]–[18], robust Direct Torque Control (DTC) and predictive control strategies for SynRM are presented, among others.

Despite a variety of control approaches can be found in the scientific literature, PI based Field Oriented Control (FOC) is one of the most commonly used torque control technique for synchronous machines [19]. This strategy must be complemented with an optimal current set point generation algorithm, which is required to drive an electric vehicle propulsion system through the maximum efficiency points, including Field Weakening (FW) operation when required. In industrial applications, in general, and commercial EV electric drives, in particular, it is of common practice to precalculate these set points and store them in Look-up tables (LUTs) [20]–[25]. The machine electrical parameters must be identified in order to calculate the aforementioned LUTs. FEM analysis [26], [27] or experimental procedures [27], [28] are usually employed, from where electric machine d- and q-axis fluxes are obtained. Permanent magnet flux and d- and q-axis inductances can be calculated from these fluxes. However, it is important to point out that an adequate mathematical approach must be followed [27].

In contrast, other strategies follow a stator flux reference frame control approach [29], or perform the optimum set point calculations in real time from inductances and PM-flux data [19], or by using estimated parameters [30], [31].

LUT based methods are commonly preferred in industry due to their low computational burden and simplicity. However, LUT approaches tune the control algorithm for an specific set of electrical parameters and may eventually loss control under parameter variations due to an incorrect FW regulation, i.e., exceeding the stator voltage limit and leading to an uncontrolled energy regeneration [32]. The high non-linearities caused by the magnetic saturation effect [27] together with electrical parameter variations due to machine ageing, manufacture tolerances and temperature dependency confirm the importance of relying on a robust control strategy that ensures the correct operation of the EV drive during its whole life-cycle.

In this paper, a robust control algorithm for EVs and/or HEVs mounting PM-Assisted SynRMs is fully designed and tested. An improvement of the LUT based FOC scheme, consisting of a second order current Sliding Mode Control (SMC) and a robust hybrid LUT/feedback based set point current generator, is proposed. The main advantage resides on the fact that optimized LUT values are used unless parameter deviations jeopardize the stator voltage limit. The current setpoint LUT data is calculated in order to minimize the copper losses at low speeds and magnetic losses at high speeds. The SMC control technique has been selected among other control strategies because of its robustness against parameter variations (which can be significant in automotive PM-assisted SynRM drives).

In the following, the machine mathematical model and the proposed control algorithm are presented. Finally, experimental results obtained in a full scale EV drive platform of 51 kW that validate the control approach are presented.

II. PM-Assisted SynRM electromagnetic model and operation constraints

Taking magnetic saturation phenomena into account, the dq synchronous reference frame stator voltage equations of the PM-assisted SynRM can be expressed as:

$$v_d = R_s i_d + \frac{d\Psi_d(i_d, i_q)}{dt} - P\omega_m \Psi_q(i_d, i_q), \tag{1}$$

$$v_q = R_s i_q + \frac{d\Psi_q(i_d, i_q)}{dt} + P\omega_m \Psi_d(i_d, i_q), \tag{2}$$

where R_s is the stator resistance, w_m is the mechanical speed, P is the pole-pair number and the current dependant magnetic fluxes are:

$$\Psi_d(i_d, i_q) = L_d(i_d, i_q) i_d + \Psi_{pm}(i_d, i_q), \tag{3}$$

$$\Psi_q(i_d, i_q) = L_q(i_d, i_q) i_q, \tag{4}$$

being $L_d(i_d, i_q)$ and $L_q(i_d, i_q)$ the current dependant inductances and being the flux of the rotor permanent magnets $\Psi_{pm}(i_d, i_q)$ relatively small. The electromagnetic torque can be expressed as:

$$T_{em} = \frac{3}{2} P(\mathbf{\Psi} \times \mathbf{i}), \tag{5}$$

being $\mathbf{\Psi} = (\Psi_d, \Psi_q)$, $\mathbf{i} = (i_d, i_q)$.

Similar to a conventional PMSM drive, a PM-Assisted SynRM drive exhibits speed and torque constraints due to inverter current rating and available DC-link voltage. These limitations must be taken into consideration [21] and can be expressed in terms of current and voltage as follows:

$$\sqrt{i_d^2 + i_q^2} \leq I_{max}, \tag{6}$$

$$L_d^2(i_d, i_q) \left[i_d + \frac{\Psi_{pm}}{L_d(i_d, i_q)} \right]^2 + L_q^2(i_d, i_q) i_q^2 \leq \left(\frac{V_{max}}{P w_m} \right)^2, \tag{7}$$

being I_{max} and V_{max} the maximum allowable stator current and voltage, respectively. In some cases, the stator resistance R_s can have a significant impact in the voltage limit expressed by (7) and must be considered. However, the effect of R_s has been neglected in this particular application because its influence is low, as $R_s = 1.74\ m\Omega$ and $I_{max} = 255\ A$.

According to these constraints, four optimum operation regions are distinguished [19], [21], [33]: Maximum Torque Per Ampere (MTPA, figure 1 region I), FW region without and with torque reduction (figure 1 regions II and III, respectively) and Maximum Torque per Volt (MTPV, figure 1 region IV). In the MTPA region, the ohmic losses (predominant at low speeds) are minimized, while in the MTPV region the magnetic losses (predominant at high speeds) are minimized.

III. Proposed robust SynRM control strategy

Figure 2 shows the general diagram of the proposed robust control strategy. In the following, the main blocks that constitute the controller, i.e. the current regulators and the set point determination strategies are presented.

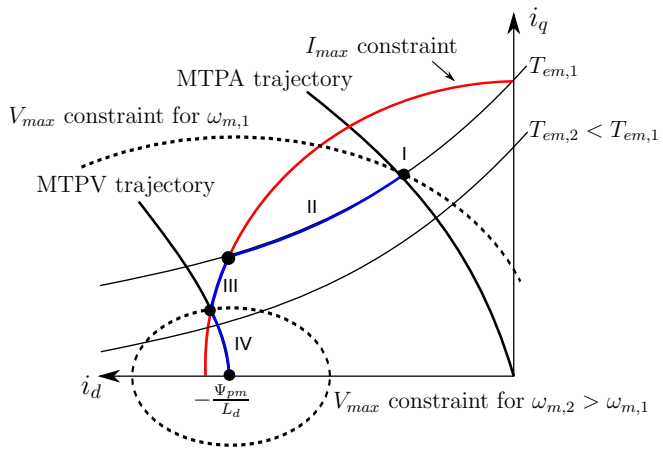

Fig. 1. Optimum control trajectories of a PM-Assisted SynRM.

A. Second order SMC current regulators

Although first order SMC can be considered as an appropriate solution for controlling electric drives connected to switching power converters [34], [35], this technique has the disadvantage of producing a variable switching frequency, which is not usually a desirable feature. Application of second order SMC allows to retain the robustness characteristics of the first order SMC control algorithm at a fixed switching frequency. Additionally, possible chatter can be reduced [36].

The SMC approach consists of two steps [34]: a) selection of a sliding surface (s) to where the system states are driven (when the state trajectory is constrained on it, $s = 0$, the controlled plant exhibits the desired performance) and b) design of a discontinuous state-feedback capable of forcing the system state to reach, in finite time, the aforementioned surface.

Aiming to achieve satisfactory tracking performance for i_d and i_q, the following sliding functions are adopted [36]:

$$s_{i_d} = e_{i_d} + c_d \int e_{i_d} dt, \tag{8}$$

$$s_{i_q} = e_{i_q} + c_q \int e_{i_q} dt, \tag{9}$$

where $e_{i_d} = (i_d^* - i_d)$ and $e_{i_q} = (i_q^* - i_q)$, being c_d and c_q positive constants. The integral terms of (8) and (9) are incorporated to remove steady state errors that may arise in practice. Satisfactory tracking is achieved when $ds_{i_j}/dt = 0$, being $j = \{d, q\}$.

Taking the time derivative of the sliding functions, the following space state expressions are obtained:

$$\frac{ds_{id}}{dt} = \frac{d}{dt}(i_d^* - i_d) + c_d e_{i_d}, \tag{10}$$

$$\frac{ds_{iq}}{dt} = \frac{d}{dt}(i_q^* - i_q) + c_q e_{i_q}. \tag{11}$$

where $d(i_d^*)/dt = d(i_q^*)/dt = 0$ considering constant current references. Using (10) and (11), the motor dynamics can be rewritten as:

$$\frac{ds_{id}}{dt} = -\frac{(-R_s i_d + w_e \Psi_q)}{L_d} - \frac{v_{d,eq}}{L_d} + c_d e_{i_d}, \tag{12}$$

$$\frac{ds_{iq}}{dt} = -\frac{(-R_s i_q - w_e \Psi_d)}{L_q} - \frac{v_{q,eq}}{L_q} + c_q e_{i_q}. \tag{13}$$

The equivalent control signals $v_{d,eq}$ and $v_{q,eq}$ can be obtained forcing $ds_{i_d}/dt = 0$ and $ds_{i_q}/dt = 0$ in (12) and (13). The voltages to be applied in the stator should be derived according to the following control law [36]:

$$v_d = v_{d,ST} + v_{d,eq}, \tag{14}$$

$$v_q = v_{q,ST} + v_{q,eq}, \tag{15}$$

where terms $v_{d,ST}$ and $v_{q,ST}$ are computed applying the Super-Twisting Algorithm (STA) [37]:

$$v_{j,ST} = L_j \left[\lambda_j |s_{i_j}|^{1/2} sgn(s_{i_j}) + \Omega_j \int sgn(s_{i_j}) dt \right], \tag{16}$$

where λ_j and Ω_j are positive gains to be tuned, being $j = \{d, q\}$ and $sgn(s_{i_j}) = s_{i_j}/|s_{i_j}|$. The goal of the first terms of (16) is to guarantee that the sliding surfaces $s_{i_d} = 0$ and $s_{i_q} = 0$ are reached at finite time. The selection of c_d, c_q and the tunning equations to correctly adjust the STA are detailed in [36].

Equivalent voltages are not strictly necessary for the second order SMC. However, they include a number of benefits: a) they improve the system's transient response, b) the more accurately they are calculated, the lower is the control effort left to the STA algorithm, c) although equivalent voltage parameters are machine parameter dependant, they do not decrease the control algorithm robustness, as it relies on the STA [36], and d) their incorporation simplifies the calculation of the sliding function constants c_d and c_q, as well as the STA constants λ_d, λ_q, Ω_d and Ω_q.

In order to consider the PM-Assisted SynRM magnetic saturation phenomena, equivalent voltages of (14) and (15) are calculated estimating the inductances $\tilde{L}_d$, $\tilde{L}_q$ and the magnetic fluxes $\tilde{\Psi}_d$, $\tilde{\Psi}_q$ from LUTs containing FEM data of such parameters (figure 2). Current references i_d^* and i_q^* have been used for parameter estimation, instead of measured values, in order to avoid feedback noise transmission to the control signals. In order to improve the drive performance at high speeds, the required phase advance has been applied to the SMC output voltage inverse Park transformation electrical angle (figure 2):

$$\theta_e' = \theta_e + 1.5 \omega_e T_s, \tag{17}$$

being T_s the control execution period.

B. Hybrid current set point generation strategy

In the absence of significant parameter mismatches, the usage of precalculated LUTs that contain the optimal current set points for the whole operation range is ideal. The dimensions required to obtain i_d^* and i_q^* in a LUT based approach depends on the specific application. Although the usage of

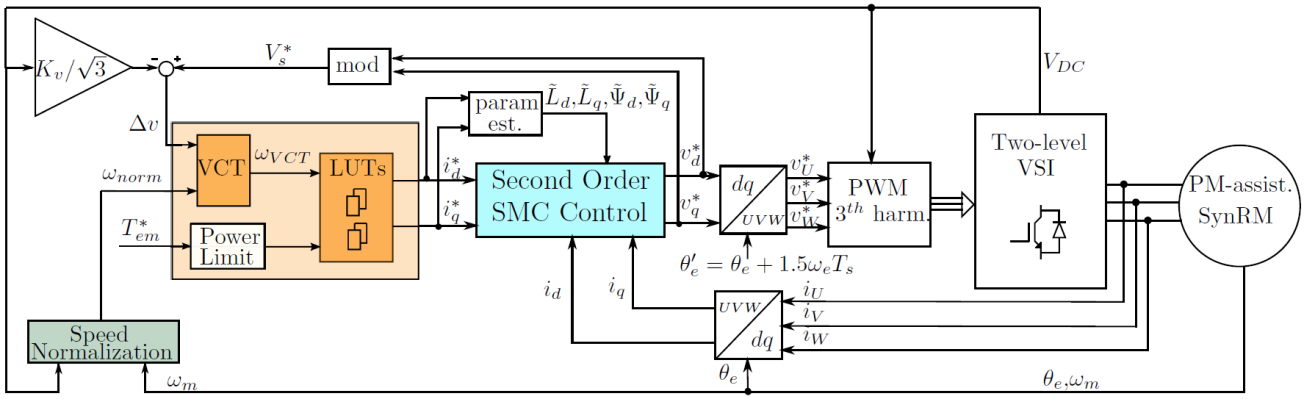

Fig. 2. General diagram of the proposed SMC with hybrid LUT/VCT based feedback control strategy.

the torque reference as an input is mandatory, the mechanical speed must also be considered in systems where FW operation is required. Additionally, DC link voltage feedback is also required in systems where V_{DC} can vary, as is the case of a battery powered EVs or HEVs. However, this magnitude can be eliminated from the LUT using the speed normalization (w_{norm}) concept [38], where the mechanical speed w_m is related to the DC-link voltage V_{DC} as (figure 3):

$$\omega_{norm} = \frac{1}{\mu}|\omega_m| = \frac{V_{DC}^{norm}}{V_{DC}}|\omega_m|, \tag{18}$$

being V_{DC}^{norm} the normalized voltage for which the current set point LUTs have been calculated.

It becomes clear that i_d^* and i_q^* depend on the machine electrical parameters. From (7), it can be derived that variations in ~~the stator resistance and~~ d- and q- axis inductances affect directly the voltage limit ellipse (figure 1), leading to possible controllability problems in FW and MTPV operation.

Conventional FW compensators only consider i_d current modification to elude the voltage limit curve, not relying on the i_q current [38], [39]. The d- and q-axis currents are coupled in the MTPV region, being the trajectory calculation a complex task. In [40], an optimized field weakening strategy is proposed, where either i_d^* or the phase angle of the reference current Γ^* are the voltage loop control actions. The corresponding transfer function is defined, allowing the precise design and adjustment of the voltage control loop. The regulator is designed considering constant electrical parameters and DC link voltage. Additional control blocks would be required in order to control a machine in MTPV mode and guarantee a smooth transition between FW and MTPV regions.

Reference [32] deals with this issue applying a Linear FW Control (LFC), i.e., the MTPV curve is linearized, simplifying the relationship between i_d and i_q currents. In contrast, in [29] a unified direct-flux vector control approach is implemented in the stator flux reference frame, allowing robust MTPV operation. This strategy requires a stator flux observer and an additional PI for MTPV current limitation. However, if the precalculated LUT data is to be maintained, the approach presented in [33] can be incorporated to the SMC control structure (figure 3) in order to improve the robustness of the SynRM torque control. Thanks to this, current references i_d^*, i_q^* are simultaneously modified throughout the regulation of the normalized mechanical speed ω_{norm} (figure 3).

Following this approach, the normalized speed of (18) is controlled using a Voltage Constraint Tracking (VCT) regulator, which aims to maintain the stator voltage vector close to the voltage limit margin in the FW and MTPV regions according to the error produced between the second order SMC regulator reference voltage V_s^* and the voltage limit V_{max}:

$$\Delta v = V_s^* - K_v V_{max} = \sqrt{(v_d^*)^2 + (v_q^*)^2} - K_v \frac{V_{DC}}{\sqrt{3}}, \tag{19}$$

where K_v provides a security margin ($K_v < 1$) in order to ensure that the voltage limit is never reached.

The normalized speed modified by the VCT algorithm in the k instant is defined by:

$$\omega_{VCT}(k) = \omega_{norm}(k) + \delta\omega(k), \tag{20}$$

being

$$\delta\omega(k) = \delta\omega(k-1) + \alpha\Delta v, \tag{21}$$

where α is a positive constant and $\delta\omega(k)$ is a correction term, saturated as follows:

$$\delta\omega(k) = \begin{cases} 0 & if\ \delta\omega(k) \leq 0, \\ \delta\omega(k) & if\ \delta\omega(k) > 0. \end{cases} \tag{22}$$

When the inverter output voltage exceeds the maximum voltage limit ($\Delta v > 0$) including the security margin, the term $\delta\omega(k)$ becomes positive, increasing the value of $\omega_{VCT}(k)$ until the voltage error Δv becomes zero. Therefore, the dq current set points are simultaneously modified (the reference current vector is maintained within the voltage ellipse constraint) in order to maintain the stator voltage in the voltage limit curve. In contrast, when the inverter output voltage is not saturated ($\Delta v \leq 0$), the correction term $\delta\omega(k)$ is negative. Taking into account the saturation effect defined in (22), the corrector term does not affect the normalized speed, and $\omega_{VCT}(k) = \omega_{norm}(k)$.

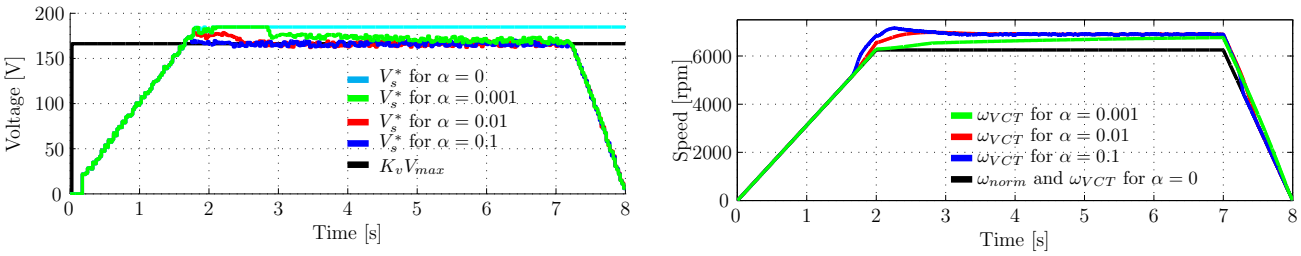

(a) Stator voltage V_s control for various values of α.

(b) w_{norm} vs w_{VCT} for various values of α.

Fig. 4. Simulation results carried out for α parameter adjustment.

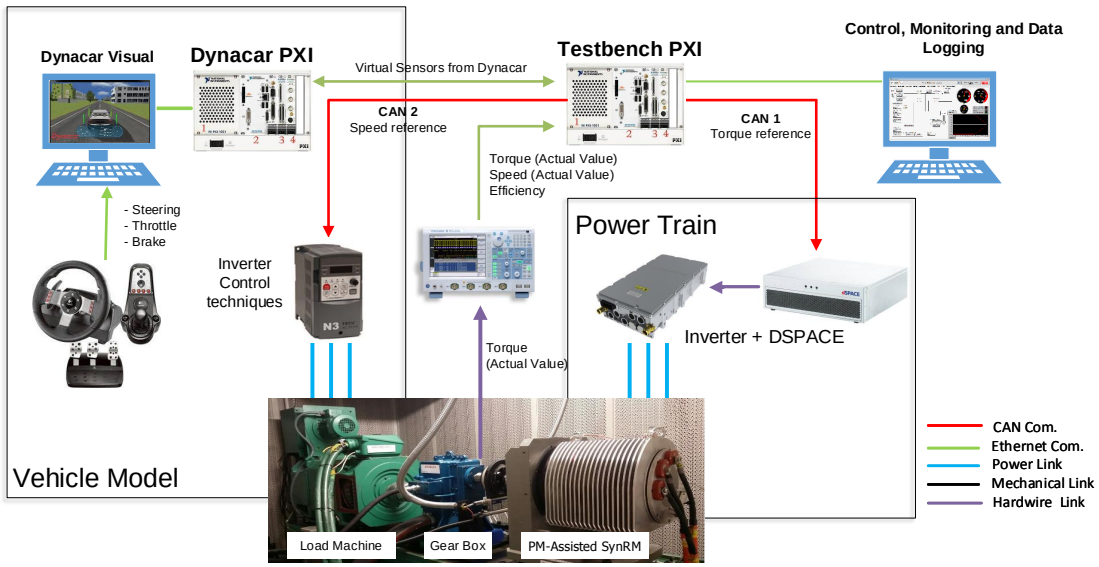

Fig. 5. Electric drive test bench overview.

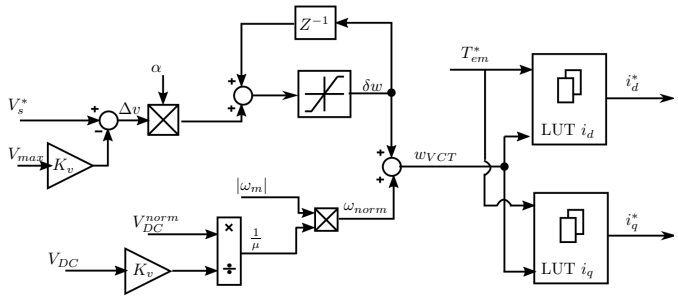

Fig. 3. Diagram of the hybrid LUT/VCT current setpoint generator with VCT based FW feedback control.

The main advantage of the proposed method relies on the fact that it only modifies the theoretically or experimentally predefined optimum set points when it is required, maintaining the LUT values when deviations are sufficiently small to ensure machine controllability.

Another benefit of this approach relies on the fact that, apart from the current regulators, only an additional control parameter (α) must be adjusted. Additionally, the added computational burden of the proposed strategy is low.

In order to adjust the VCT regulation parameter α, simulations have been carried out considering $\pm 10\%$ errors in the SynRM electrical parameters (figure 4). As it can be seen from figure 4, the system losses control if no VCT regulation is achieved ($\alpha = 0$), driving V_s^* into saturation. Taking into account the EV drive dynamics and according to simulation, a value of α between 0.01 and 0.1 has been considered for its fine tuning in the experimental platform.

IV. Experimental Results

A. Experimental platform description

In this section, experimental results that validate the proposed SynRM control strategy are presented. Tests have been carried out in the automotive test bench of figure 5, which is constituted by the following main elements:

- A counter-load IM of a maximum speed of 8000 rpm and maximum power of 157 kW that emulates the electric vehicle behavior.
- A 1:1.8 gearbox that allows a maximum speed up to 14400 rpm for the machine under test.
- A modular dSPACE Rapid Control Prototyping device, equipped with a slot-CPU control board (DS1006) and an AC Motor Control Solutions board.

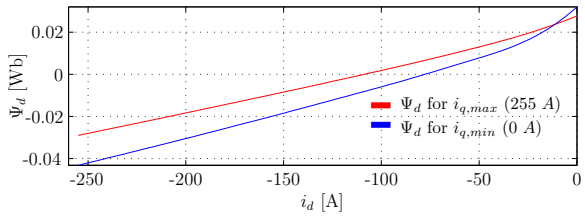

(a) Flux Ψ_d for minimum and maximum q-axis currents

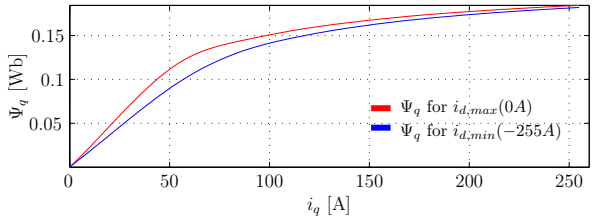

(b) Flux Ψ_q for minimum and maximum d-axis currents

Fig. 6. PM-Assisted SynRM d and q ~~inductances~~ fluxes according to FEM analysis.

TABLE I
NOMINAL PARAMETERS OF THE PM-ASSISTED SYNRM.

Item	Symbol	Value	Units
Maximum power	P_N	51	kW
Maximum speed	w_{max}	12000	rpm
Machine Pole Pairs	P	3	-
Stator Resistance	R_s	1.74	mΩ
d-axis nominal inductance	L_d	0.7	mH
q-axis nominal inductance	L_q	1.7	mH
Permanent Magnet Flux linkage	Ψ_{pm}	0.38	Wb
Stator nominal current	I_{nom}	255	A
DC-link nominal voltage	$V_{DC,nom}$	320	V

- Complete road vehicle real time model (DYNACAR®) including both longitudinal and lateral car dynamics to emulate real driving conditions.
- An industrial Semikron IGD-1-424-P1N4-DL-FA power inverter, with a nominal power of 140 kW and a maximum switching frequency of 25 kHz.
- An HBM HBMT40B torquimeter.

The proposed control strategy has been validated in a 51 kW automotive PM-Assisted SynRM, whose most significant parameters are listed in Table I. Taking into account the nature of this machine, the effects of magnetic saturation and cross coupling in the machine's electrical behavior have an important impact and cannot be neglected. The d- and q-axis ~~inductances and ferrite magnets flux~~ magnetic fluxes obtained throughout Finite Element Model (FEM) analysis are shown in figure 6. The switching frequency of the converter has been set to 10 kHz. A dead-time compensation algorithm [41] has been carried out in order to minimize its effect. The optimal current set point LUTs have been precalculated using the FEM data of the machine. The control dynamics requirements and the SMC parameters used for this application are listed in Table II.

TABLE II
SMC PARAMETER SETTINGS.

Target control dynamics		
Item	**Symbol**	**Value**
Damping coefficient	ξ	1
Settling time	T_s	10 ms
$c_{d,q}$ selection and STA parameters		
Item	**Symbol**	**Value**
Sliding function parameters	$c_{d,q}$	580
STA parameter Ω	$\Omega_{d,q}$	$1.682e^5$
STA parameter λ	$\lambda_{d,q}$	$2.8532e^3$
VCT parameters		
Item	**Symbol**	**Value**
DC-link voltage security margin	k_v	0.9
VCT positive constant	α	0.01

B. Experimental validation

Figure 7 shows the results of the proposed SMC control strategy when conventional LUT based approach and hybrid LUT/VCT approach are used for current set point determination, at machine maximum torque (130 Nm). The SMC current regulation is satisfactory, producing a low torque ripple. Note that, as in real EV applications, electromagnetic torque has been indirectly measured from the stator currents. If the VCT feedback is not included (figures 7(a), 7(c) and 7(e)), the stator voltage surpasses the voltage limit for a given mechanical speed, and the system is driven into an uncontrolled regeneration. This means that the maximum speed of the vehicle would be significantly reduced in a real EV application. In this particular case, the maximum machine speed of 12000 rpm corresponds to a maximum vehicle speed of 120 km/h. Taking into account that the control gets lost at around 4000 rpm, the vehicle maximum speed would be limited to 40 km/h, which would be unacceptable for the end user.

This issue is due to the fact that there are significant differences between the FEM data and the experimental machine, mainly due to the following reasons:

- No rotor temperature measurement is available. FEM analysis has been carried out for a particular set of stator winding and magnets temperatures. Therefore, the LUTs do not take into consideration the parameter variations produced by the temperature.
- Small deviations between the specified and the real airgap (due to manufacturing and mounting tolerances) highly affect the electrical parameters of the machine. This aspect is aggravated in PM-assisted SynRM machines, due to the sensitivity of ferrite magnets to this particular parameter.
- A 2.5D FEM model has been considered and, as a consequence, no information about the stray inductances of the winding heads can be obtained from the simulations. These stray inductances increase the resulting phase inductances, obtaining higher terminal voltages than expected.

However, system robustness is guaranteed when the hybrid LUT control strategy is included (figures 7(b), 7(d) and 7(f)). A robust torque and FW control performance is achieved in the whole operating range (figure 8) using the second order SMC

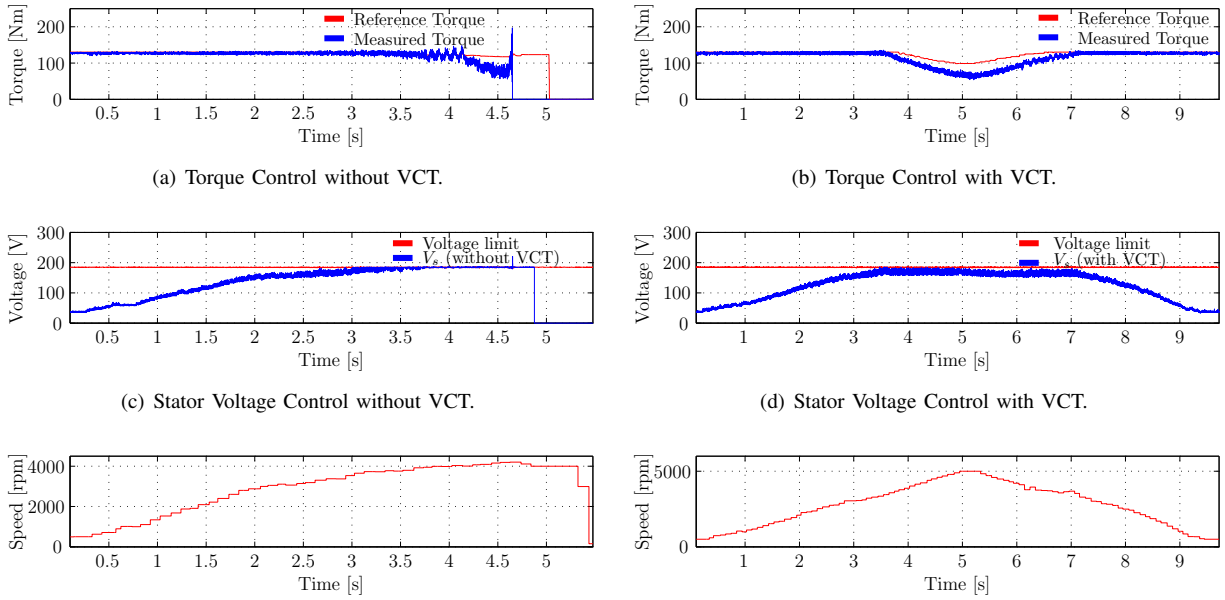

(a) Torque Control without VCT.

(b) Torque Control with VCT.

(c) Stator Voltage Control without VCT.

(d) Stator Voltage Control with VCT.

(e) Mechanical Speed.

(f) Mechanical Speed.

Fig. 7. SMC Torque control, stator voltage V_s control and mechanical speed results with and without the VCT control strategy.

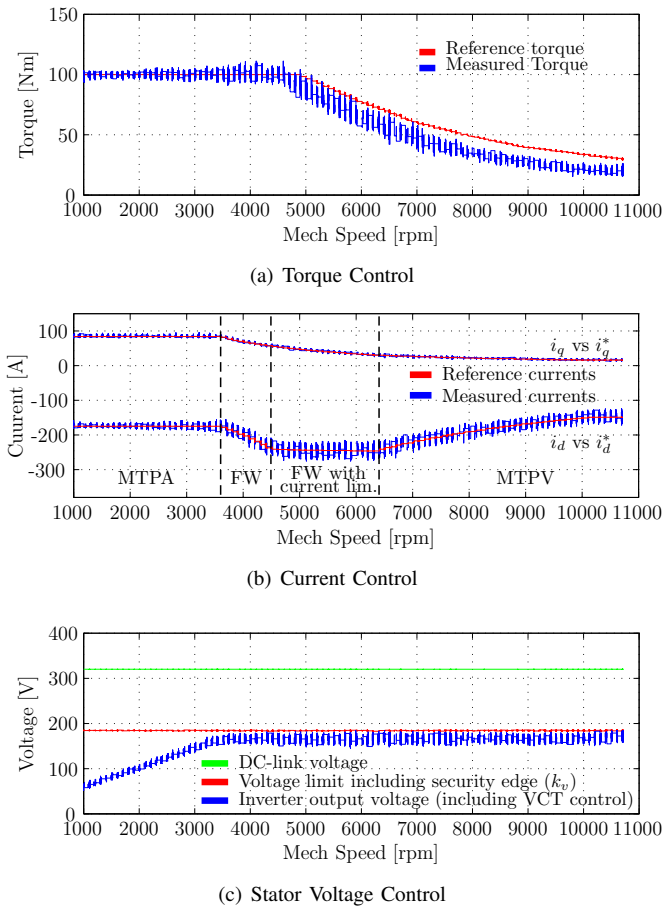

(a) Torque Control

(b) Current Control

(c) Stator Voltage Control

Fig. 8. Torque, current and stator voltage regulation ~~SMC~~ experimental results using the proposed hybrid LUT/VCT based FW strategy.

control strategy combined with the proposed optimal current set point generation. Current references are properly modified by the VCT algorithm (figure 8(b)), while torque production capability is reduced once the current limit is reached (figures 8(a) and 8(b)), and also during MTPV, in order to ensure the required voltage regulation. As it can be seen in figure 8(c), smooth transitions between the different operation regions is achieved. The corresponding current vector trajectory throughout the different operation regions in the dq plane is shown in figure 9.

The difference between the torque setpoint and the actual torque (measured using a torquimeter) reveals the aforementioned mismatch between the real electrical parameters and the ones predicted by FEM analysis, as deviations of around 15 Nm have been confirmed at constant torque region and for maximum torque setpoint.

Figure 10 shows the torque regulation for transients (in this case, torque changes from motoring to regenerative braking). Being an EV propulsion system, torque reference transients are ramped in order to improve the confort of the passengers. Both the SMC regulators and the hybrid set point generator prove to be robust in the occurrence of such torque transients. The SMC control equivalent voltages $v_{d,eq}$ and $v_{q,eq}$ are required to obtain a satisfactory transient response.

In order to evaluate the drive performance under real driving conditions, a standard Worldwide harmonized Light vehicles Test Procedure (WLTP) has been carried out. Driving cycles aim to analyze a vehicle's performance in terms of consumption, pollution and efficiency, among other factors. The WLTP is an specific driving cycle supposed to represent light duty vehicle operation and its accuracy ensures more realistic results that conventional driving cycles [42]. The latter's speed profile and torque response in both urban and extra urban

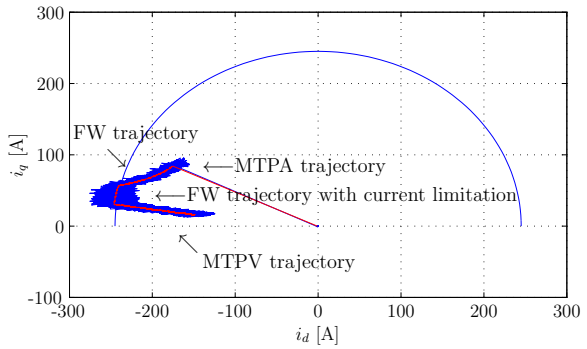

Fig. 9. Current trajectories in the dq axis (current vector reference in red; measured current vector in blue).

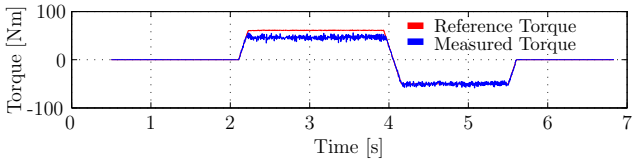

(a) Torque Control

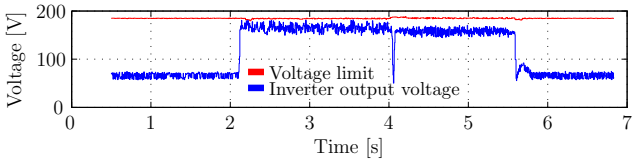

(b) Stator Voltage Control using VCT

Fig. 10. Torque control stability using VCT strategy when changing from motor driving to reverse braking t a constant speed of 7000 rpm.

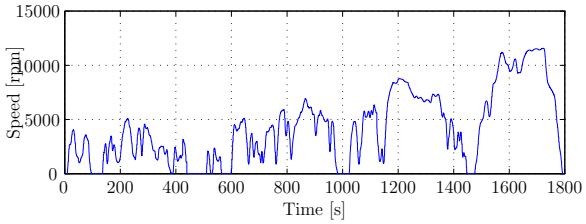

(a) Mechanical Speed

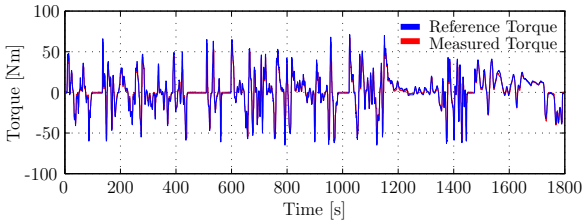

(b) Torque

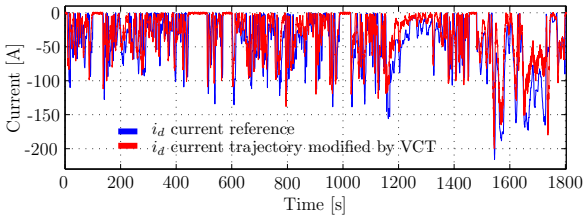

(c) VCT influence in d-axis current

Fig. 11. Worldwide harmonized Light vehicles Test Procedures (WLTP) results.

cycles are shown in figure 11, including the torque response of the SynRM machine, which satisfactorily follows the reference requested by the driving cycle. Figure 11(c) shows how the VCT feedback acts modifying the d-axis current set point when required. These results corroborate that the proposed strategy is ready to be implemented in real EVs and/or HEVs.

V. Conclusions

PM-Assisted SynRMs are promising candidates for future EV and HEV rare earth free electric drives. However, due to design aspects, the electrical parameter variability of such machines can be very high. As it has been demonstrated throughout experiments, electric parameter deviations have a high impact in the machine controllability, causing serious controllability problems in this type of drive. As a consequence, robust control strategies are required in order to ensure a satisfactory torque control.

In this paper, a robust control strategy that combines second order SMC current regulators with an optimal hybrid current set point generation algorithm has been proposed, ensuring a satisfactory torque regulation in the whole machine operation range under parameter variations. Experimental tests have been carried out in a state of the art test bench which emulates the EV and/or HEV real application, validating the proposed approach, both under speed and torque variations and also under simulated real driving conditions. It is therefore reasonable to guess that the proposed VCT would properly cope with the angle and speed estimation errors introduced by any sensorless strategy. Moreover, the proposed strategy can be easily extended to other synchronous machine types, such as pure SynRMs and PMSMs.

References

[1] J. Alsawalhi and S. Sudhoff, "Design optimization of asymmetric salient permanent magnet synchronous machines," *IEEE Transactions on Energy Conversion*, vol. 31, no. 4, pp. 1315–1324, 2016.

[2] I. Boldea, L. Tutelea, L. Parsa, and D. Dorrell, "Automotive electric propulsion systems with reduced or no permanent mmagnet: An overview," *IEEE Transactions on Industrial Electronics*, vol. 61, no. 10, pp. 5696–5711, 2014.

[3] J. Riba, C. López-Torres, L. Romeral, and A. Garcia, "Rare-earth-free propulsion motors for electric vehicles: A technology review," *Renewable and Sustainable Energy Reviews*, no. 57, pp. 367–379, 2016.

[4] T. Guo, N. Schofield, and A. Emadi, "Double segmented rotor switched reluctance machine with shared stator back-iron for magnetic flux passage," *IEEE Transactions on Energy Conversion*, vol. 31, no. 4, pp. 1278–1286, 2016.

[5] V. Vujicic and M. Casalan, "Simple sensorless control for high-speed operation of switched reluctance generator," *IEEE Transactions on Energy Conversion*, vol. 31, no. 4, pp. 1325–1335, 2016.

[6] D. Reed, H. Hofmann, and J. Sun, "Offline identification of induction machine parameters with core loss estimation using the stator current locus," *IEEE Transactions on Energy Conversion*, vol. 31, no. 4, pp. 1549–1558, 2016.

[7] P. Guglielmi, M. Pastorelli, G. Pellegrino, and A. Vagati, "Position-sensorless control of permanent-magnet-assisted synchronous reluctance motor," *IEEE Transactions on Industry Applications*, vol. 40, no. 2, pp. 615–622, 2004.

[8] C. Chen, T. Liu, and M. Lin, "Position control of a sensorless synchronous reluctance motor," *IEEE Transactions on Industrial Electronics*, vol. 51, no. 1, pp. 15–24, 2004.

[9] S. Ooi, M. Morimoto, M. Sanada, and Y. Inoue, "Performance evaluation of a high power density pmasynrm with ferrite magnets," *IEEE Transactions on Industry Applications*, vol. 49, no. 3, pp. 1308–1315, 2013.

[10] P. Reddy, K. Grace, and A. El-Refaie, "Conceptual design of sleeve rotor synchronous reluctance motor for traction applications," *IET Electric Power Applications*, vol. 10, no. 5, pp. 368–347, 2016.

[11] Y. Wang, D. Ionel, M. Jiang, and S. Stretz, "Establishing the relative merits of synchronous reluctance and pm-assisted technology through systematic design optimization," *IEEE Transactions on Industry Applications*, vol. 52, no. 4, pp. 2971–2978, 2016.

[12] N. Bianchi, S. Bolognani, E. Carraro, M. Castiello, and E. Fornasiero, "Electric vehicle traction based on synchronous reluctance motors," *IEEE Transactions on Industry Applications*, vol. 52, no. 6, pp. 4762–4769, 2016.

[13] N. Bianchi and Z. Mahmoud, "An analytical approach to design the pm in pmarel motors robust toward the demagnetization," *IEEE Transactions on Energy Conversion*, vol. 31, no. 2, pp. 800–809, 2016.

[14] M. Hinkkanen, H. Awan, Z. Qu, T. Tuovinen, and F. Briz, "Current control for synchronous motor drives: Direct discrete-time pole-placement design," *IEEE Transactions on Industry Applications*, vol. 52, no. 2, pp. 1530–1541, 2016.

[15] A. Guagnano, G. Rizzello, F. Cupertino, and D. Naso, "Robust control of high-speed synchronous reluctance machines," *IEEE Transactions on Industry Applications*, vol. 52, no. 5, pp. 3990–4000, 2016.

[16] G. Foo and X. Zhang, "Robust direct torque control of synchronous reluctance motor drives in the field-weakening region," *IEEE Transactions on Power Elect*, vol. 32, no. 2, pp. 1289–1298, 2017.

[17] R. Antonello, M. Carraro, L. Peretti, and M. Zigliotto, "Hierarchical scaled-states direct predictive control of synchronous reluctance motor drives," *IEEE Transaction on Industrial Electronics*, vol. 63, no. 8, pp. 5176–5185, 2016.

[18] C. Lin, J. Yu, Y. Lai, and H. Yu, "Improved model-free predictive current control for synchronous reluctance motor drives," *IEEE Transactions on Industrial Electronics*, vol. 63, no. 6, pp. 3942–3953, 2016.

[19] S. Jung, J. Hong, and K. Nam, "Current minimizing torque control of the ipmsm using ferrari's method," *IEEE Transactions on Power Electronics*, pp. 5603–5617, 2013.

[20] J. Lara, J. Xu, and A. Chandra, "Effects of rotor position error in the performance of field-oriented-controlled pmsm drives for electric vehicle traction applications," *IEEE Transaction on Industrial Electronics*, vol. 63, no. 8, pp. 4738–4751, 2016.

[21] S. Morimoto, Y. Takeda, T. Hirasa, and K. Taniguchi, "Expansion of operating limits for permanent magnet morot by current vector control considering inverter capacity," *IEEE Transactions on Industry Applications*, vol. 26, no. 5, pp. 866–871, 1990.

[22] G. Rang, J. Lim, K. Nam, H. Ihm, and H. Kim, "A mtpa control scheme for an ipm synchronous motor considering magnet flux variation caused by temperature," in *Applied Power Electronics Conference and Exposition (APEC)*, 2004.

[23] M. Meyer and J. Bocker, "Optimum control for interior permanent magnet synchronous motors (ipmsm) in constant torque and flux weakening range," in *EPE-PEMC Conference*, pp. 282–286, 2006.

[24] Y. Kim and S. Sul, "Torque control strategy of an ipmsm considering the flux variation of the permanent magnet," in *Industry Applications Conference*, 2007.

[25] Y. Wang, D. Ionel, V. Rallabandi, M. Jiang, and S. Stretz, "Large-scale optimization of synchronous reluctance machines using ce-fea and differential evolution," *IEEE Transactions on Industry Applications*, vol. 52, no. 6, pp. 4699–4709, 2016.

[26] K. M. Rahman and H. S, "Identification of machine parameters of a synchronous motor," *IEEE Industry Aplications (IAS) conference*, 2013.

[27] K. Meessen, P. Thelin, J. Soulard, and E. Lomonova, "Inductance calculations of permanent-magnet synchronous machines including flux change and self- and cross-saturations," *IEEE Transactions on Magnetics*, vol. 44, no. 10, pp. 2324–2331, 2008.

[28] M. Yilmaz and P. T. Krein, "Capabilities of finite element analysis and magnetic equivalent circuits for electrical machine analysis and design," *IEEE Power Electronics Specialist Conference (PESC)*, 2008.

[29] G. Pellegrino, R. Bojoi, and P. Guglielmi, "Unified direct-flux vector control for ac motor drives," *IEEE Transactions on Industry Applications*, vol. 47, no. 5, pp. 20 193–2102, 2011.

[30] H. Kim and R. Lorenz, "Improved current regulators for ipm machine drives using on-line parameter estimation," *Proc. of the IEEE Industry Applications Conference (IAS)*, 2002.

[31] D. Dang, M. Rafaq, H. Choi, and J. Jung, "Online parameter estimation technique for adaptive control applications of interior pm synchronous motor drives," *IEEE Transaction on Industrial Electronics*, vol. 63, no. 3, pp. 1438–1449, 2016.

[32] K. Chen, Y. Sun, and B. Liu, "Interior permanent magnet synchronous motor linear field-weakening control," *IEEE Transactions on Energy Conversion*, vol. 31, no. 1, pp. 159–164, 2016.

[33] E. Trancho, E. Ibarra, A. Arias, C. Salazar, I. Lopez, A. Diaz de Guereñu, and A. Peña, "Ipmsm torque control strategies based on luts and vct feedback for robust control under machine parameter variations," in *Proc. of the Industrial Electronics Society Conferece (IECON)*, 2016.

[34] A. Pisano, "Second order sliding modes: Theory and applications," Ph.D. dissertation, Dipartimento di Ingegneria Eletrica ed Elettronica, Univerista degli Studi di Cagliari, 2000.

[35] S. Liu, J. andVazquez, L. Wu, A. Marquez, H. Gao, and L. Franquelo, "Extended state observer-based sliding-mode control for three-phase power converters," *IEEE Transactions on Industrial Electronics*, vol. 64, no. 1, pp. 22–31, 2017.

[36] A. Susperregui, M. Martinez, I. Zubia, and G. Tapia, "Design and tuning of fixed-switching-frequency second-order sliding-mode controller for doubly fed induction generator power control," *IET Electric Power Applications*, vol. 6, pp. 696–706, 2012.

[37] A. Levant, "Sliding order and sliding accuracy in sliding mode control," *International Journal of Control*, vol. 58, no. 6, pp. 1247–1263, 1993.

[38] J. Lee, C. Won, B. Lee, J. Baek, K. Han, and U. Chung, "Ipmsm torque control method considering dc-link voltage variation and friction torque for ev/hev applications," in *Proc. of the IEEE Vehicle Power and Propulsion Conference*, pp. 1063–1069, 2012.

[39] J. Kim and S. Sul, "Speed control of interior permanent magnet synchronous motor drive for the flux weakening operation," *IEEE Transactions on Industry Applications*, vol. 33, no. 1, pp. 43 – 48, Jan. 1997.

[40] S. Bolognani, S. Calligaro, and R. Petrella, "Adaptive flux-weakening controller for interior permanent magnet synchronous motor drives," *IEEE Journal of Emerging and Selected Topics in Power Electronics*, vol. 2, no. 2, pp. 236–248, 2014.

[41] J. L. Lin, "A new approach of dead-time compensation for pwm voltage inverters," *IEEE Transactions on Circuits and Systems - I: Fundamental Theory and Applications*, vol. 49, no. 4, 2002.

[42] U. Tietge, N. Zacharof, P. Mock, V. Franco, J. German, B. A., N. Ligterink, and U. Lambrecht, "A 2015 update of official and real-world fuel consumption and co 2 values for passenger cars in europe," *The International Council of Clear Transportation*, 2015.